Scientific Research Publishing

Journal of Applied Mathematics and Physics, 2026, 14(3), 1218-1243
https://www.scirp.org/journal/jamp
ISSN Online: 2327-4379
ISSN Print: 2327-4352

Optimization Method for Distribution Locational Marginal Pricing Considering Stepped Carbon Trading and Source-Grid-Load-Storage Coordination

Haolong Wu

School of Management, University of Shanghai for Science and Technology, Shanghai, China
Email: 18110236810@163.com

How to cite this paper: Wu, H.L. (2026) Optimization Method for Distribution Locational Marginal Pricing Considering Stepped Carbon Trading and Source-Grid-Load-Storage Coordination. *Journal of Applied Mathematics and Physics*, **14**, 1218-1243.
https://doi.org/10.4236/jamp.2026.143058

Received: March 2, 2026
Accepted: March 16, 2026
Published: March 19, 2026

Abstract

The high penetration of distributed energy resources (DERs) exacerbates net load fluctuations in distribution networks. Existing dynamic pricing research often ignores complex physical constraints, yielding dispatch outcomes that are "mathematically optimal yet physically infeasible". To address this, we propose a day-ahead optimal dispatch and pricing strategy that jointly considers AC power flow constraints and a stepped carbon trading mechanism. We establish a market framework—integrating distributed generation, energy storage, and electric vehicle aggregators—to reinforce low-carbon incentives. A continuous second-order cone programming (SOCP) relaxation is employed to address power flow non-convexity, ensuring strict adherence to voltage and line security limits. Based on duality theory, the Distribution Locational Marginal Price (DLMP) is analytically derived to comprehensively internalize the spatial-temporal marginal costs of energy, congestion, losses, and carbon emissions. Simulations on a modified IEEE 33-bus system demonstrate that these spatiotemporally differentiated price signals effectively guide flexible resources to mitigate voltage and congestion risks. Compared to traditional fixed pricing, the proposed DLMP mechanism maximizes social welfare by unlocking higher user utility and rationally internalizing environmental costs, validating its effectiveness in fostering the low-carbon synergistic optimization of "Source-Grid-Load-Storage".

Keywords

Social Welfare Maximization, Distribution Locational Marginal Pricing (DLMP), Stepped Carbon Trading, Electric Vehicles (EVs), Second-Order Cone Programming (SOCP)

1. Introduction

Driven by "dual carbon" goals, power systems are rapidly shifting toward the high-proportion integration of renewable energy sources (RES) [1] [2]. As the critical interface with end-users, distribution networks face significant challenges from the massive penetration of distributed energy resources (DERs). Specifically, the volatility of RES output increases power flow complexity, risking voltage violations and network congestion [3] [4]. Furthermore, traditional dispatch modes struggle to accommodate massive flexible resources, necessitating a shift toward collaborative "source-network-load-storage" interaction [5] [6]. Consequently, designing market mechanisms that balance economic efficiency, physical security, and low-carbon objectives has emerged as a core focus in smart grid research.

In demand-side management (DSM), real-time pricing (RTP) is recognized as a highly efficient incentive mechanism [7]. Compared to traditional pricing, locational marginal pricing (LMP) accurately reflects the spatial marginal value of energy, congestion, and loss costs, seeing wide application in transmission markets [8] [9]. This theory has naturally extended to distribution networks as distribution locational marginal pricing (DLMP) [10], which guides users to avoid congested periods and enhances operational efficiency. While existing studies have utilized DLMP to resolve stakeholder conflicts [11] and transmission-distribution coordination [3], the high resistance-to-reactance ratio of distribution networks renders traditional dc power flow models inapplicable [12]. To address the nonconvexity of nonlinear ac power flow, second-order cone programming (SOCP) relaxation effectively handles DistFlow constraints, guaranteeing global optimality [13] [14].

Despite advancements in physical modeling, current DLMP frameworks lack refined low-carbon incentives. Most clearing models target economic cost or social welfare [15] [16]. Even when carbon taxes are introduced, they are often treated as fixed parameters, ignoring the spatial-temporal dynamics of emissions. Although "electricity-carbon coupling" pricing has been proposed to transfer emission responsibilities [17], the dynamic impact of tiered incentives on nodal prices remains underexplored. Tiered carbon pricing sensitively reflects marginal emission costs through segmented penalties, proving effective in integrated energy systems, yet its integration into DLMP remains rare.

Additionally, coordinating electric vehicles (EVs) and distributed energy storage systems (ESSs) is vital for smoothing net load fluctuations [18] [19]. Many studies employ game-theoretic bi-level models [20] [21] or reinforcement learning [22] for source-load interactions. However, these methods often suffer from slow convergence when handling large-scale nodes and complex constraints, failing RTP's timeliness requirements. In contrast, centralized optimization based on social welfare maximization (SWM) combined with convex relaxation offers superior computational efficiency and global optimality [23]-[26].

To bridge these gaps, this paper proposes an optimization strategy for DLMP considering tiered carbon trading and source-load-storage coordination. Specifi-

cally, a distribution network SWM model integrating RES, independent ESS, and EV aggregators is established. By linearizing the tiered carbon pricing mechanism, dynamic emission components are directly incorporated into nodal prices. Furthermore, SOCP technology relaxes nonconvex DistFlow constraints, transforming the model into a solvable convex second-order cone programming (SOCP) problem that ensures voltage and power flow security. Finally, the DLMP is analytically derived via duality theory. Serving as a comprehensive price signal that reflects the marginal costs of energy, network congestion, losses, and carbon emissions, its effectiveness in optimizing resource allocation, alleviating congestion, and achieving the optimal trade-off between economic utility and environmental costs is validated through numerical case studies.

2. System Framework

This paper constructs a market architecture for a low-carbon active distribution network (ADN) based on social welfare maximization (SWM), as illustrated in Figure 1. Physically anchored on the IEEE 33-node radial network, the system encompasses diverse entities, including the distribution system operator (DSO), distributed renewable energy sources (RES), independent energy storage systems (ESS), electric vehicle (EV) aggregators, and load aggregators. Serving as the core administrator and open platform of the regional market, the DSO facilitates bidirectional energy transactions with the upstream main grid via the point of common coupling (PCC). Additionally, it gathers comprehensive data on network loads, RES forecasts, and line parameters to safeguard physical security and execute unified market clearing. Meanwhile, EV aggregators and independent ESSs participate as critical flexible resources. Specifically, EV aggregators represent decentralized vehicles equipped with vehicle-to-grid (V2G) capabilities. Operating as price takers, they respond to price signals for arbitrage while strictly satisfying users' travel demands. Conversely, independent ESSs are strategically deployed at critical nodes, receiving dispatch commands to smooth renewable energy fluctuations and mitigate line congestion.

To realize the low-carbon and economic collaborative dispatch of the "source-network-load-storage" paradigm, a unified pricing mechanism internalizing tiered carbon costs is designed. First, the DSO introduces a tiered carbon trading mechanism by establishing baseline emission quotas. The nonlinear penalty costs for emissions exceeding these quotas are directly integrated into the objective function, thereby explicitly reflecting the environmental value of carbon within electricity prices. Following this, built upon the SWM model subject to DistFlow constraints, second-order cone programming (SOCP) relaxation is employed to secure the global optimum. Distribution locational marginal pricing (DLMP) is then analytically derived using duality theory. Functioning as a comprehensive economic signal that reflects the marginal variations in energy supply, network security, and carbon emissions, the DLMP naturally guides all market participants to autonomously optimize their strategies.

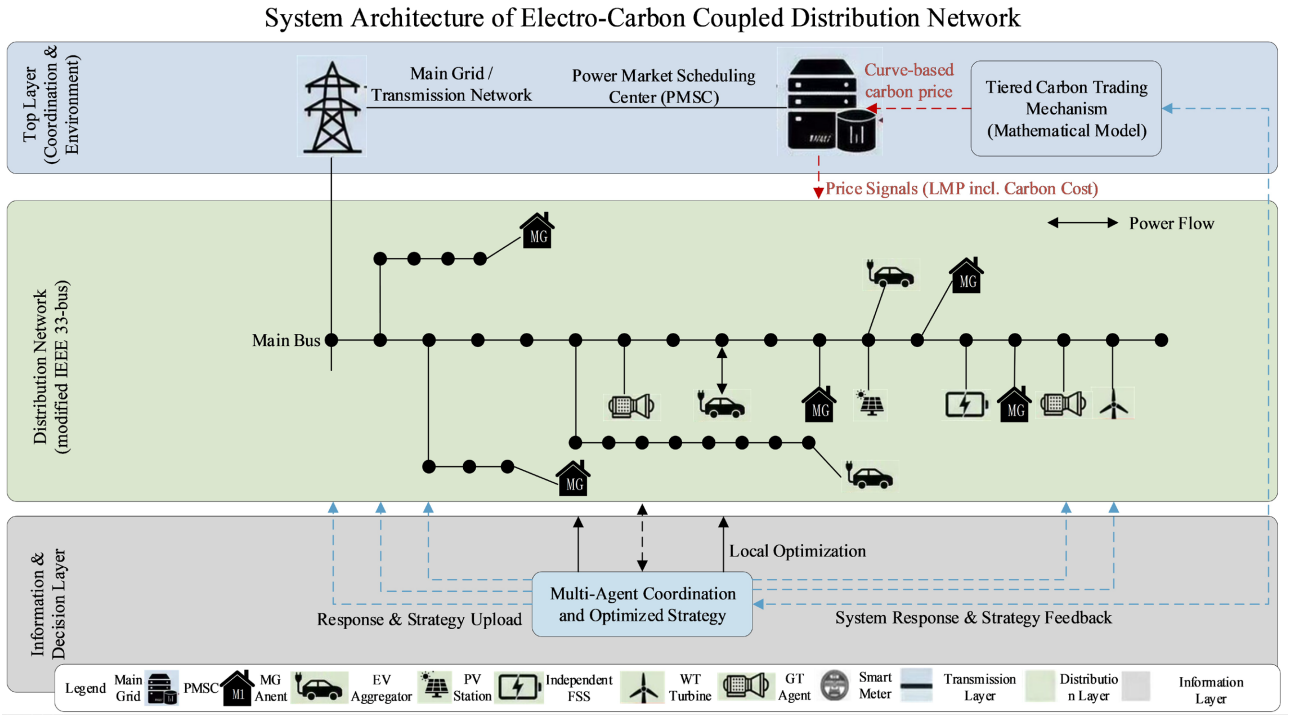

Figure 1. System structure diagram.

3. System Modeling

This section adopts a modular modeling approach to construct the operational models of various market participants in the distribution network. Combined with physical network constraints, a global optimization model for maximizing social welfare is ultimately formulated.

3.1. Load Aggregator Modeling

As the resource agent of node i, the load aggregator (LA) smooths out individual randomness and reduces the dispatch dimensionality through the aggregated management of decentralized users within its jurisdiction. To clarify the dispatch boundaries, the total nodal load $P_{load,i,t}$ is decoupled into a rigid base load $P_{fix,i,t}$ and a flexible load $P_{flex,i,t}$. The former is rigidly integrated as a known parameter, while the latter participates in the optimization as a decision variable. Following the principle of diminishing marginal utility in microeconomics, the LA aims to maximize the aggregated electricity consumption utility of the flexible load. It is expressed using a convex quadratic function as follows [7]:

$$U_{LA,i,t} = \omega_i P_{flex,i,t} - \frac{\alpha}{2}\left(P_{flex,i,t}\right)^2 \tag{1}$$

where ω_i and α are the aggregated utility parameters of node i, representing the users' initial marginal willingness to consume electricity and the rate of diminishing marginal utility, respectively.

While pursuing utility maximization, the actual adjustment amount of the flexible load is limited by the rated power of the aggregator's physical equipment and

the nodal power balance constraints:

$$0 \le P_{flex,i,t} \le P_{flex,i}^{max} \tag{2}$$

$$P_{load,i,t} = P_{fix,i,t} + P_{flex,i,t} \tag{3}$$

where $P_{flex,i}^{max}$ is the upper limit of the adjustable power for the flexible load at node i.

3.2. EV Aggregator Modeling

Serving as an intermediary between the distribution network and decentralized vehicle owners, the electric vehicle (EV) aggregator employs Minkowski sum theory to equivalently model the highly stochastic EV fleet within its jurisdiction as a virtual energy storage unit equipped with vehicle-to-grid (V2G) capabilities [2]. To quantify the uncertainties associated with vehicle integration, the model introduces the number of online vehicles $N_{i,t}$, the arrival energy $E_{arr,i,t}$, and the inflexible departure energy demand $E_{dep,i,t}$ as known parameters. These parameters are generated via Monte Carlo simulations based on probability distributions of residential travel behavior. The objective of the aggregator is to minimize its operational cost, which is primarily driven by battery degradation life loss during charging and discharging cycles. According to electrochemical characteristics, this cost is approximated as a quadratic function of power:

$$C_{EV,i,t} = \alpha_{ev}\left[\left(P_{ch,i,t}^{ev}\right)^2 + \left(P_{dis,i,t}^{ev}\right)^2\right] \tag{4}$$

where $P_{ch,i,t}^{ev}$ and $P_{dis,i,t}^{ev}$ are decision variables representing the charging and discharging power of the aggregator, respectively; and α_{ev} is the battery degradation coefficient.

On the physical operation front, the energy state of the aggregator is not solely governed by charging and discharging actions; it must also satisfy the dynamic energy balance constraints induced by the random arrival and departure of vehicles:

$$E_{i,t+1}^{ev} = E_{i,t}^{ev}\left(1-\delta\right) + \eta_{ch}P_{ch,i,t}^{ev}\Delta t - \frac{P_{dis,i,t}^{ev}}{\eta_{dis}}\Delta t + E_{arr,i,t} - E_{dep,i,t} \tag{5}$$

Simultaneously, the regulation capacity of the aggregator exhibits time-varying properties, with its power and capacity boundaries strictly constrained by the volume of online vehicles at any given time:

$$0 \le P_{ch,i,t}^{ev} \le N_{i,t}P_{single}^{max} \tag{6}$$

$$0 \le P_{dis,i,t}^{ev} \le N_{i,t}P_{single}^{max} \tag{7}$$

$$N_{i,t}E_{single}^{min} \le E_{i,t}^{ev} \le N_{i,t}E_{single}^{max} \tag{8}$$

where δ is the self-discharge rate; η_{ch} and η_{dis} are the charging and discharging efficiencies, respectively; and P_{single}^{max} and $E_{single}^{min/max}$ denote the rated power and capacity boundaries of a single vehicle, respectively. By incorporating the E_{dep} term into the constraints, the model inherently guarantees that the users' travel

energy requirements are fulfilled upon grid disconnection.

3.3. Energy Storage System Modeling

As a flexible resource with a fixed location and defined capacity in the distribution network, the independent energy storage system (ESS) utilizes its time-shifting characteristics—charging during off-peak periods and discharging during peak periods—to smooth renewable energy fluctuations and alleviate line congestion. Unlike EVs, the ESS is not constrained by the randomness of traffic behavior; its operational state is primarily determined by its own physical capacity and electrochemical characteristics. Under a market-oriented operating environment, the dispatch strategy of the ESS depends on the trade-off between arbitrage revenues and battery degradation costs. To quantify the impact of frequent charging and discharging on the storage lifespan, this paper adopts a battery degradation cost function based on the square of power:

$$C_{ESS,k,t} = \alpha_{ess}\left[\left(P^{ess}_{ch,k,t}\right)^2 + \left(P^{ess}_{dis,k,t}\right)^2\right] \tag{9}$$

where α_{ess} is the degradation coefficient of the storage unit; $P^{ess}_{ch,k,t}$ and $P^{ess}_{dis,k,t}$ are decision variables representing the charging and discharging power of the energy storage, respectively.

The physical operation of the ESS must strictly comply with the law of energy conservation. The time evolution of its state of charge (SOC) is jointly determined by the energy at the previous time step, the charging and discharging power, and the self-discharge loss. Furthermore, it must satisfy the energy consistency constraint between the initial and final periods to ensure cycle sustainability:

$$E^{ess}_{k,t+1} = E^{ess}_{k,t}\left(1-\delta\right) + \eta_{ch}P^{ess}_{ch,k,t}\Delta t - \frac{P^{ess}_{dis,k,t}}{\eta_{dis}}\Delta t \tag{10}$$

$$E^{ess}_{k,0} = E^{ess}_{k,T} \tag{11}$$

Simultaneously, the charging and discharging behaviors of the storage system must be strictly restricted within the safety thresholds of its converter's rated power and battery capacity:

$$0 \le P^{ess}_{ch,k,t} \le P^{ess,max}_{k} \tag{12}$$

$$0 \le P^{ess}_{dis,k,t} \le P^{ess,max}_{k} \tag{13}$$

$$E^{ess,min}_{k} \le E^{ess}_{k,t} \le E^{ess,max}_{k} \tag{14}$$

where $P^{ess,max}_{k}$ is the maximum charging and discharging power; and $E^{ess,min/max}_{k}$ denote the allowable lower and upper bounds of the battery capacity.

3.4. Distributed Renewable Energy Modeling

Distributed renewable energy sources (RES) primarily encompass wind turbines (WT) and photovoltaics (PV). To scientifically handle the stochastic nature of their output in the dispatch model, this paper adopts a modeling strategy of "pa-

rameters defining boundaries, variables determining outputs". Based on the statistical distributions of historical meteorological data (Weibull distribution for wind speed and Beta distribution for solar irradiance), Monte Carlo simulations are utilized to generate the maximum available power $P_{WT,i,t}^{max}$ and $P_{PV,i,t}^{max}$ at each time interval as known parameter inputs. The marginal cost of RES is mainly composed of operation and maintenance (O&M) expenses, generating zero carbon emissions. The model characterizes its cost using a linear function to economically incentivize the prioritized consumption of clean energy:

$$C_{RES,t} = \sum_{w \in \Omega_{WT}} c_{om}^{WT} P_{WT,w,t} + \sum_{v \in \Omega_{PV}} c_{om}^{PV} P_{PV,v,t} \tag{15}$$

where c_{om} is the O&M coefficient per unit of electrical energy; and Ω_{WT} and Ω_{PV} are the sets of wind and photovoltaic units, respectively.

Constrained by resource endowments and the physical accommodation capacity of the distribution network, the actual dispatched output of RES (decision variables) must be adjusted between zero and the maximum available power. This implies permitting necessary wind and solar curtailment under extreme operating conditions such as network congestion:

$$0 \le P_{WT,w,t} \le P_{WT,w,t}^{max} \tag{16}$$

$$0 \le P_{PV,v,t} \le P_{PV,v,t}^{max} \tag{17}$$

where $P_{WT,w,t}^{max}$ and $P_{PV,v,t}^{max}$ are known parameters representing the theoretical maximum available power of wind turbines and photovoltaic units at time t, respectively, based on meteorological conditions.

3.5. Traditional Distributed Generation Modeling

Traditional distributed generation (DG) primarily refers to controllable fossil fuel power generation equipment, such as micro gas turbines, acting as key resources for peak shaving and valley filling in distribution networks. Their generation cost primarily depends on fuel consumption. According to thermodynamic characteristics, the model employs a convex quadratic function to describe their operational costs. The operational cost $C_{DG,g,t}$ of unit g located at node i at time t is defined as:

$$C_{DG,g,t} = a_g \left(P_{g,i,t}\right)^2 + b_g P_{g,i,t} + c_g \tag{18}$$

where $P_{g,i,t}$ is the actual output of the unit; and a_g, b_g, and c_g are the fuel cost coefficients. This quadratic feature linearly increases the unit's marginal cost as output rises, aligning with economic dispatch principles.

On the physical operational level, the dispatch of DG must simultaneously satisfy steady-state capacity limits and dynamic ramping constraints. Specifically, the unit's output must be maintained within the technically permissible safety zone, and the power adjustment rate between adjacent periods is restricted by mechanical inertia and thermal stress, preventing sudden mutations. The aforementioned physical constraints can be uniformly formulated as:

$$P_g^{min} \le P_{g,i,t} \le P_g^{max} \tag{19}$$

$$-R_g^{down} \le P_{g,i,t} - P_{g,i,t-1} \le R_g^{up} \tag{20}$$

where P_g^{min} and P_g^{max} are the minimum technical output and rated capacity of the unit, respectively; and R_g^{up} and R_g^{down} are the maximum upward and downward ramping rates of the unit. This set of constraints ensures that dispatch instructions are executed strictly within the unit's physical feasible region.

3.6. Grid Interaction Modeling

The distribution network achieves bidirectional energy exchange with the upstream main grid through the point of common coupling (PCC). As a price taker, the DSO adjusts its interaction strategy based on real-time price signals issued by the upstream grid. Considering the asymmetry between purchasing and selling electricity prices in actual power markets (*i.e.*, the purchasing price $\lambda_{buy,t}$ is usually higher than the selling price $\lambda_{sell,t}$), the model decouples the net exchange power at the PCC into two nonnegative decision variables to precisely quantify interaction costs and avoid nonconvexity: power purchased from the grid $P_{buy,t}$ and power sold to the grid $P_{sell,t}$. Based on this, the net operational cost resulting from grid interaction is defined as the difference between electricity purchasing expenditures and selling revenues:

$$C_{Grid,t} = \lambda_{buy,t} P_{buy,t} - \lambda_{sell,t} P_{sell,t} \tag{21}$$

where $\lambda_{buy,t}$ and $\lambda_{sell,t}$ are known parameters representing the selling price and recovery price of the main grid at time t, respectively.

On the physical operational level, the bidirectional interaction power must be strictly limited within the thermal stability transmission limits of the tie-line transformers and lines to guarantee system security:

$$0 \le P_{buy,t} \le P_{grid}^{max} \tag{22}$$

$$0 \le P_{sell,t} \le P_{grid}^{max} \tag{23}$$

where P_{grid}^{max} is the maximum allowable transmission power of the PCC tie-line. The difference between these two decision variables, $P_{buy,t} - P_{sell,t}$, will be substituted into the subsequent network power flow equations as the injected power at the source node to maintain the energy balance of the entire network.

3.7. Tiered Carbon Trading Mechanism

To embed environmental costs into the economic dispatch, the model introduces a tiered carbon trading mechanism. Unlike unified system-wide accounting, this paper adopts a hierarchical carbon responsibility mechanism: the carbon emission costs of distributed generation (DG) are internalized within their marginal generation costs and borne by the operators themselves, whereas the distribution system operator (DSO) is primarily evaluated on the indirect carbon emissions generated from purchasing electricity from the upstream main grid.

The real-time net carbon emissions $E_{net,t}$ on the DSO side are defined as the

net value of carbon emissions generated from main grid electricity purchases minus the baseline free quota:

$$E_{net,t} = \mu_{grid} P_{buy,t} \Delta t - E_{quota} \tag{24}$$

$$E_{quota} = \eta_{quota} \sum_{t=1}^{T} P_{buy,t} \Delta t \tag{25}$$

where μ_{grid} is the average carbon emission factor of the upstream grid; E_{quota} is the free carbon quota based on the total purchased electricity; and η_{quota} is the quota coefficient.

Addressing the net emissions E_{net} (typically accumulated over the daily dispatch cycle), the DSO introduces a segmented auxiliary variable $E_{aux,m}$ to linearize the nonlinear tiered costs. Assuming the total number of tiers is M, the interval length of the m-th tier is L_m, and the corresponding carbon price is $\lambda_{c,m}$, the carbon trading cost C_{Carbon} is expressed as:

$$C_{Carbon} = \sum_{m=1}^{M} \lambda_{c,m} E_{aux,m} \tag{26}$$

$$\begin{aligned} \text{s.t.} \quad & \sum_{t=1}^{T} E_{net,t} \le \sum_{m=1}^{M} E_{aux,m} \\ & 0 \le E_{aux,m} \le L_m, \quad \forall m = 1, \cdots, M \end{aligned} \tag{27}$$

This mechanism increases the operational costs of high-carbon emission behaviors through progressively increasing marginal carbon prices, thereby effectively incentivizing the system to prioritize the consumption of clean energy on an economic level.

3.8. Distribution Network Safety Constraints

The physical power flow of the distribution network must adhere to Kirchhoff's laws. For the radial network structure, this paper adopts the branch power flow model (DistFlow) to describe the coupling relationship between nodal voltages and branch powers [27]. For line ij, its active power flow $P_{ij,t}$, reactive power flow $Q_{ij,t}$, the square of the nodal voltage magnitude $U_{i,t}$, and the square of the branch current magnitude $l_{ij,t}$ must satisfy the following physical balance equations:

$$\sum_{k \in \delta(j)} P_{jk,t} = P_{ij,t} - r_{ij} l_{ij,t} + P_{inj,j,t} \tag{28}$$

$$\sum_{k \in \delta(j)} Q_{jk,t} = Q_{ij,t} - x_{ij} l_{ij,t} + Q_{inj,j,t} \tag{29}$$

$$U_{j,t} = U_{i,t} - 2\left(r_{ij} P_{ij,t} + x_{ij} Q_{ij,t}\right) + \left(r_{ij}^2 + x_{ij}^2\right) l_{ij,t} \tag{30}$$

where r_{ij} and x_{ij} are the resistance and reactance parameters of the line, respectively; $\delta(j)$ is the set of downstream nodes; and $P_{inj,j,t}$ and $Q_{inj,j,t}$ are the net injected active and reactive power (difference between source and load) at node j, respectively. It is worth noting that the exactness of the second-order cone programming (SOCP) relaxation is theoretically guaranteed under the radial topology of the distribution network and the proposed objective function [28]

[29]. Since the social welfare maximization objective implicitly drives the system to minimize total operational costs and active power losses, the optimization naturally forces the relaxed inequalities to be strictly active (*i.e.*, binding tight as an equality). This structural property perfectly prevents the generation of fictitious losses and ensures the physical feasibility of the AC power flow.

To address the nonconvexity of $l_{ij,t}U_{i,t} = P_{ij,t}^2 + Q_{ij,t}^2$ in the original power flow equations, the model introduces second-order cone programming (SOCP) relaxation technology, transforming it into a rotated second-order cone constraint. Furthermore, it sets safety thresholds for nodal voltages and line currents to safeguard the physical security of the system:

$$l_{ij,t}U_{i,t} \geq P_{ij,t}^2 + Q_{ij,t}^2 \tag{31}$$

$$\left(V_{min}\right)^2 \leq U_{i,t} \leq \left(V_{max}\right)^2 \tag{32}$$

$$0 \leq l_{ij,t} \leq \left(I_{max,ij}\right)^2 \tag{33}$$

where V_{min} and V_{max} are the allowable lower and upper bounds of nodal voltage fluctuations, respectively; and $I_{max,ij}$ is the thermal stability current limit of the line. The aforementioned constraints constitute the feasible region boundary of the optimization model, ensuring that the dispatch results satisfy the security and stability of the physical network.

3.9. Global Social Welfare Maximization Model

Integrating the operational characteristics of the market participants and the physical model of the distribution network described above, this paper constructs a day-ahead optimal dispatch model with the objective of social welfare maximization (SWM). This model aims to discover the global optimal solution that balances user-side utility and system operational costs by coordinating source, load, storage, and grid resources. Its complete mathematical description is as follows:

$$\max SW = \sum_{t=1}^{T}\left\{\sum_{i\in\Omega_{Load}} U_{LA,i,t} - \left[C_{EV,t} + C_{ESS,t} + C_{RES,t} + C_{DG,t} + C_{Grid,t} + C_{Carbon,t}\right]\right\} \tag{34}$$

s.t.

$$\begin{aligned} P_{inj,i,t} = {} & P_{WT,i,t} + P_{PV,i,t} + P_{g,i,t} + P_{dis,i,t}^{ess} - P_{ch,i,t}^{ess} \\ & + P_{dis,i,t}^{ev} - P_{ch,i,t}^{ev} + P_{buy,i,t} - P_{sell,i,t} - P_{load,i,t} \end{aligned} \tag{35}$$

$$Q_{inj,i,t} = Q_{WT,i,t} + Q_{PV,i,t} + Q_{g,i,t} + Q_{ess,i,t} + Q_{ev,i,t} - Q_{load,i,t} \tag{36}$$

$$\begin{aligned} \boldsymbol{x} \in \Omega = \{ & (2)\text{-}(3),(5)\text{-}(8),(10)\text{-}(14),(16)\text{-}(17), \\ & (19)\text{-}(20),(22)\text{-}(23),(26)\text{-}(27),(28)\text{-}(33)\} \end{aligned} \tag{37}$$

The objective function (34) comprehensively considers the economic efficiency and utility of the entire network. The first term represents the flexible electricity consumption utility of the load aggregator, defined by Equation (1); the cost terms within the brackets sequentially denote: the battery degradation cost $C_{EV,t}$ of the EV aggregator defined by Equation (4); the operational degradation cost $C_{ESS,t}$

of the independent ESS defined by Equation (9); the operation and maintenance cost $C_{RES,t}$ of renewable energy defined by Equation (15); the fuel cost $C_{DG,t}$ of traditional distributed generation defined by Equation (18); the net electricity purchasing cost $C_{Grid,t}$ generated from main grid interaction defined by Equation (21); and the tiered trading cost $C_{Carbon,t}$ for the portion of system carbon emissions exceeding the quota, defined by Equation (25).

The constraint set Ω encompasses the network's physical balance and the operational boundaries of each entity. Specifically, (35)-(36) are the nodal active and reactive power balance equations, serving as the physical ties linking source, load, storage, and the grid; (2)-(3) are the upper and lower bounds for the flexible regulation of the load aggregator; (5)-(8) are the energy evolution and charging/discharging capacity constraints for the EV aggregator; (10)-(14) are the state of charge and capacity boundary constraints for the independent ESS; (16)-(17) are the maximum available output constraints for wind and photovoltaic renewable energy; (19)-(20) are the output intervals and ramping rate constraints for traditional generation units; (22)-(23) are the transmission capacity constraints for the tie-line at the PCC; (26)-(27) are the linearization constraints for the tiered carbon trading mechanism; and (28)-(33) constitute the DistFlow network security constraints based on SOCP relaxation, safeguarding that nodal voltages and line currents remain within safe perimeters. The aforementioned model is a typical convex optimization problem. According to microeconomic principles, the dual variables of Equation (35) correspond to the distribution locational marginal pricing (DLMP) at each node. Based on the Lagrangian dual decomposition theory, this paper will subsequently utilize a distributed iterative algorithm to solve it.

4. Model Solving and Distributed Pricing Mechanism

The social welfare maximization model constructed in Chapter 3 belongs to a convex optimization problem involving second-order cone constraints. Given that this problem involves profit interactions among multiple entities and includes power balance constraints coupled across the entire network, solving it centrally makes it difficult to guarantee the privacy and security of various market participants. Although centralized clearing can mathematically yield the exact optimal prices under strict convexity, a distributed implementation pathway is more practical in real-world electricity markets. Therefore, based on the Lagrangian dual decomposition theory, this chapter constructs a dual problem by relaxing the coupling constraints, transforming the global optimization into a distributed solving framework through collaborative iteration between the DSO and various aggregators, and subsequently deriving the DLMP that reflects real-time supply and demand relationships.

4.1. Construction of Lagrangian Dual Function

Define the system-wide decision variable vector $\boldsymbol{x}$ as the set of control variables for all market participants, *i.e.*, $\boldsymbol{x} = \{P_{flex}, P_{ev}, P_{ess}, P_{res}, P_{dg}, P_{grid}\}$. The core cou-

pling term in the original model is the nodal active power balance equation (35), while the remaining constraints (e.g., physical equipment boundaries, network security constraints, and reactive power balance) only involve the internal variables of each entity, constituting the local feasible region Ω of their respective subsystems.

A Lagrangian multiplier vector $\boldsymbol{\lambda} = \left[\lambda_{i,t}\right]_{N\times T}$ corresponding to the active power balance constraint of node i at time t is introduced. By relaxing this coupling constraint into the objective function, the partial Lagrangian function $L(\boldsymbol{x}, \boldsymbol{\lambda})$ is constructed as follows:

$$L(\boldsymbol{x}, \boldsymbol{\lambda}) = \sum_{t=1}^{T} \left\{ F_{SW}(\boldsymbol{x}_t) - \sum_{i\in\Omega_N} \lambda_{i,t} \cdot \left(P_{inj,i,t}(\boldsymbol{x}_t)\right) \right\} \tag{38}$$

where F_{SW} is the original objective function (34); and $P_{inj,i,t}$ is the expression for nodal net injected active power (*i.e.*, the algebraic sum of source and load) defined by Equation (35). Under this framework, the optimal solution to the original problem is equivalent to the solution of the following dual problem:

$$\min_{\boldsymbol{\lambda}} \max_{x\in\Omega} L(\boldsymbol{x}, \boldsymbol{\lambda}) \tag{39}$$

where Ω is the Cartesian product feasible region formed by all other formulas (2)-(34) and (36)-(37), excluding the active power balance constraint (35). The physical significance of the dual variable $\lambda_{i,t}$ is exactly the optimal locational marginal price (DLMP) capable of clearing the market. This dual problem will be solved through alternating iterations, with the DSO updating the price $\boldsymbol{\lambda}$ and each entity optimizing its variable $\boldsymbol{x}$ within its local feasible region Ω.

4.2. Decomposition of Distributed Sub-Problems

Based on the separable characteristics of the Lagrangian function $L(\boldsymbol{x}, \boldsymbol{\lambda})$, the global optimization problem can be decomposed into N independent optimization sub-problems for market participants and 1 network verification sub-problem for the DSO. Under the condition of a given active power price signal $\boldsymbol{\lambda}^{(k)}$ at the k-th iteration, the mathematical models of the sub-problems are as follows:

4.2.1. Load Aggregator (LA) Sub-Problem

The LA aims to maximize its net electricity consumption utility. In its objective function, the first term is the users' flexible electricity consumption utility defined by Equation (1), and the second term is the electricity purchasing cost calculated based on the current electricity price. Constraints (2)-(3) define the regulation boundaries for curtailable and shiftable loads:

$$\begin{gathered} \min \sum_{t=1}^{T} \left[-U_{LA,i,t} + \lambda_{i,t}^{(k)} P_{flex,i,t} + \frac{\rho}{2} \left(P_{flex,i,t} - P_{flex,i,t}^{(k-1)} \right)^2 \right] \\ \text{s.t. } (2)\text{-}(3) \end{gathered} \tag{40}$$

4.2.2. Electric Vehicle (EV) and Energy Storage System (ESS) Sub-Problems

These entities aim to exploit temporal price differences, minimizing their total

operational costs (including battery degradation and electricity purchasing expenditures) by optimizing charging and discharging strategies. For the EV aggregator, the first term of the objective function is the battery life degradation cost defined by Equation (4), and the second term is the net transaction cost generated by charging and discharging; constraints (5)-(8) stipulate the battery capacity, charging/discharging power, and users' travel demand limits:

$$\begin{aligned} &\min \sum_{t=1}^{T}\left[C_{EV,i,t}+\lambda_{i,t}^{(k)}P_{net,i,t}^{ev}+\frac{\rho}{2}\left(P_{net,i,t}^{ev}-P_{net,i,t}^{ev(k-1)}\right)^2\right] \\ &P_{net}^{ev}=P_{dis}-P_{ch} \\ &\text{s.t.}\quad (5)\text{-}(8) \end{aligned} \tag{41}$$

For the independent energy storage system, the meanings of the terms in the objective function are similar to those of the EV, and its physical operation must satisfy the state of charge and capacity constraints defined by Equations (10)-(14):

$$\begin{aligned} &\min \sum_{t=1}^{T}\left[C_{ESS,k,t}+\lambda_{i,t}^{(k)}P_{net,k,t}^{ess}+\frac{\rho}{2}\left(P_{net,k,t}^{ess}-P_{net,k,t}^{ess(k-1)}\right)^2\right] \\ &P_{net}^{ess}=P_{dis}-P_{ch} \\ &\text{s.t.}\quad (10)\text{-}(14) \end{aligned} \tag{42}$$

4.2.3. Distributed Generation (RES & DG) Sub-Problem

Generation-side resources encompass traditional units and renewable energy, both of which formulate their bidding strategies based on price signals. For traditional distributed generation (DG), its objective is to maximize net profit. Additionally, DG must bear the direct carbon emission costs resulting from its generation, which have been internalized into its marginal operational cost coefficients. The objective function consists of generation costs (Equation (18)) and electricity sales revenues; constraints (19)-(20) limit its physical output boundaries:

$$\begin{aligned} &\min \sum_{t=1}^{T}\left[C_{DG,g,t}^{total}-\lambda_{i,t}^{(k)}P_{g,i,t}+\frac{\rho}{2}\left(P_{g,i,t}-P_{g,i,t}^{(k-1)}\right)^2\right] \\ &\text{s.t.}\quad (19)\text{-}(20) \end{aligned} \tag{43}$$

For renewable energy sources (RES), the RES aggregator determines its bidding output based on the price signal, considering the operation and maintenance costs defined in Equation (15). Although it typically operates at maximum power, it can actively curtail output when network congestion leads to low electricity prices. This sub-problem encompasses the sets of wind and photovoltaic units Ω_{RES}, and the decision variables must satisfy the maximum available power constraints defined by Equations (16)-(17):

$$\begin{aligned} &\min \sum_{t=1}^{T}\left[C_{RES,t}-\sum_{r\in\Omega_{RES}}\lambda_{i,t}^{(k)}P_{r,i,t}+\frac{\rho}{2}\sum_{r\in\Omega_{RES}}\left(P_{r,i,t}-P_{r,i,t}^{(k-1)}\right)^2\right] \\ &\text{s.t.}\quad (16)\text{-}(17) \end{aligned} \tag{44}$$

4.2.4. DSO Network Security Checking Sub-Problem

The DSO is responsible for maintaining the physical security of the distribution

network and managing main grid interactions. Its objective is to minimize the system operational costs, which include net expenditures on main grid purchases and sales (the first term, Equation (21)) and the indirect tiered carbon trading costs caused by main grid electricity purchases (the second term, Equation (25)), minus the virtual congestion surplus collected from various aggregators (the third term). The feasible region Ω_{DSO} for this problem is constituted by main grid interaction limits, carbon quota constraints, and network-wide power flow security constraints, incorporating the nodal reactive power balance Equation (36) to ensure the physical feasibility of system voltage solutions:

$$\begin{aligned} &\min \sum_{t=1}^{T}\left[C_{Grid,t}+C_{Carbon,t}^{grid}-\sum_{i\in\Omega_N}\lambda_{i,t}^{(k)}P_{inj,i,t}^{DSO}+\frac{\rho}{2}\sum_{i\in\Omega_N}\left(P_{inj,i,t}^{DSO}-P_{inj,i,t}^{DSO(k-1)}\right)^2\right] \\ &\text{s.t.}\quad \boldsymbol{x}_{DSO}\in\Omega_{DSO}=\{(22)\text{-}(23),(26)\text{-}(27),(28)\text{-}(33),(36)\} \end{aligned} \tag{45}$$

where $\boldsymbol{x}_{DSO}$ is the set of internal decision variables for the DSO, covering PCC interaction power, line power flows, and nodal voltage states.

4.3. Distributed Iterative Algorithm Based on Proximal ADMM

Given the non-smoothness and large-scale nonconvex constraints (DistFlow) of the dual problem (39), traditional subgradient methods often converge slowly and are prone to oscillations. To this end, this paper adopts the Proximal Alternating Direction Method of Multipliers (Proximal ADMM) for the solution. By introducing a quadratic penalty term into the augmented Lagrangian function, ADMM effectively smooths the dual function, enhancing the robustness and convergence speed of the algorithm.

4.3.1. Construction of Augmented Lagrangian Function

A quadratic penalty factor $\rho>0$ is introduced to construct the augmented Lagrangian function $L_\rho(\boldsymbol{x},\boldsymbol{\lambda})$ as follows:

$$\begin{aligned} L_\rho(\boldsymbol{x},\boldsymbol{\lambda}) &= \sum_{t=1}^{T}F_{obj}(\boldsymbol{x}_t)+\sum_{t=1}^{T}\sum_{i\in\Omega_N}\lambda_{i,t}\left(P_{inj,i,t}(\boldsymbol{x}_t)-P_{load,i,t}\right) \\ &+\frac{\rho}{2}\sum_{t=1}^{T}\sum_{i\in\Omega_N}\left\|P_{inj,i,t}(\boldsymbol{x}_t)-P_{load,i,t}\right\|_2^2 \end{aligned} \tag{46}$$

where the third term is a quadratic regularization term used to penalize behaviors violating the power balance constraint, forcing the system to rapidly converge toward a feasible solution.

4.3.2. Algorithm Execution Process

Step 1: System Initialization

The DSO sets the parameter ρ, the maximum number of iterations K_{max}, and the precision tolerance ϵ. The electricity price $\boldsymbol{\lambda}^{(1)}$ is initialized.

Step 2: Primal Update

Each entity (LA, EV, ESS, DG, DSO) solves its local sub-problem containing the quadratic proximal term in parallel. Taking the LA as an example, its objective

function is modified to:

$$\min \sum_{t=1}^{T}\left[C_{LA}-\lambda_{i,t}^{(k)}P_{flex}+\frac{\rho}{2}\left(P_{flex}-P_{flex}^{(k-1)}\right)^{2}\right] \tag{47}$$

Step 3: Primal Residual Calculation

The DSO collects the net injected power reported by all parties and calculates the nodal power imbalance (primal residual):

$$\xi_{i,t}^{(k+1)}=P_{inj,i,t}^{(k+1)}-P_{load,i,t} \tag{48}$$

Step 4: Dual Update

The DSO utilizes the residual to update the nodal electricity price. Unlike the subgradient method, the update step size of ADMM is fixed as ρ:

$$\lambda_{i,t}^{(k+1)}=\lambda_{i,t}^{(k)}+\rho\cdot\xi_{i,t}^{(k+1)} \tag{49}$$

Step 5: Convergence Check

If $\left\|\boldsymbol{\xi}^{(k+1)}\right\|_{2}\le\epsilon$, the algorithm terminates.

5. Case Study

To verify the effectiveness of the proposed mechanism, numerical simulations are conducted based on a modified IEEE 33-node distribution network system. The system's base capacity is set to 10 MVA, and the base voltage is 12.66 kV. The simulation period covers a 24-hour dispatch horizon with a time resolution of 1 hour ($\Delta t=1\,\mathrm{h}$). The optimization problem is formulated as a continuous second-order cone programming (SOCP) model. While Section 4 designs a theoretical distributed market-clearing framework based on Proximal ADMM to preserve the data privacy of market entities, the fundamental economic outcomes—such as social welfare and locational prices—are mathematically equivalent under both centralized and distributed solving modes due to the strict convexity of the SOCP model. Therefore, to rigorously benchmark the optimal economic dispatch and focus on analyzing the pricing properties, the case study directly solves the centralized SOCP global optimization model using the Gurobi solver within the MATLAB 2021b environment.

5.1. Simulation Setup

The distribution network is interconnected with the main grid through the point of common coupling at node 1, with a bidirectional interaction power limit of 5 MW. The system integrates two dispatchable distributed gas turbines with distinct operational characteristics, connected to node 10 and node 25, respectively. Their detailed capacity and cost parameters are listed in Table 1. Regarding renewable energy sources, a photovoltaic station and a wind turbine are integrated at node 18 and node 33, respectively, both possessing a rated capacity of 0.8 MW. Their normalized daily output curves, generated from historical data, are illustrated in Figure 2.

Table 1. Relevant parameters of generator sets.

Unit No	Capacity (MW)	Min Output (MW)	a (CNY/MW²h)	b (CNY/MWh)	c (CNY/h)
unit1	0.6	0	50	600	10
unit2	1.0	0.15	60	750	20

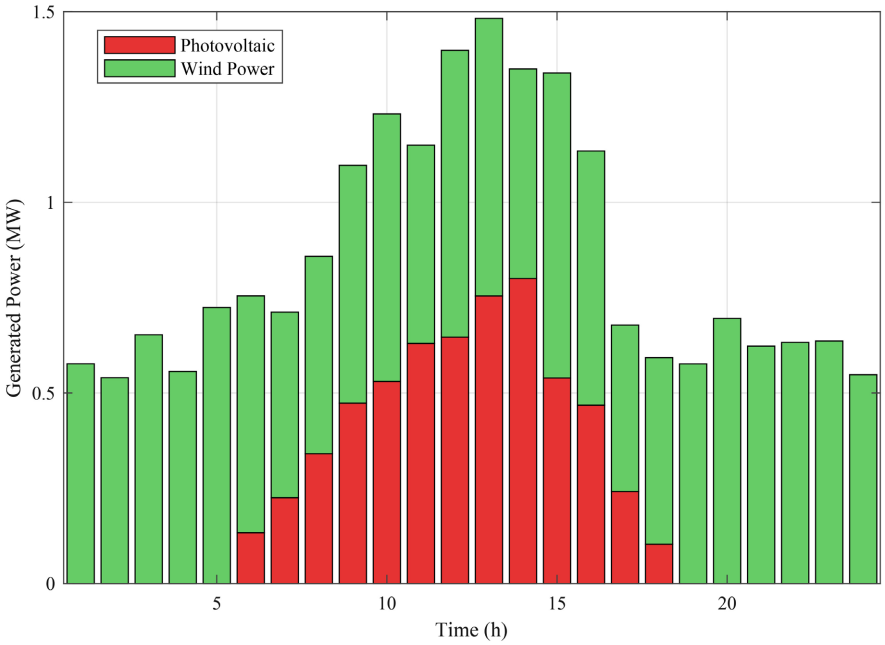

Figure 2. Forecasted power generation of distributed renewable energy sources.

The demand side comprises three load aggregators located at nodes 7, 24, and 30. Their utility functions follow Equation (1), where the willingness-to-pay parameter ω varies within the interval [2] [6] depending on the load type, and the elasticity coefficient α is set to 0.1. Furthermore, an independent energy storage system is deployed at node 15 to provide flexibility support. Its rated power is 0.6 MW, its energy capacity is 2.0 MWh, and both charging and discharging efficiencies are 95%. The electric vehicle aggregator, modeled at node 22, manages a fleet of 60 EVs within its jurisdiction. To simulate real-world travel characteristics, a heterogeneous vehicle fleet is constructed, consisting of commuting (40%), daytime working (20%), night shift (20%), and random (20%) behavior patterns. This paper employs Monte Carlo simulations to generate the dispatchable capacity boundaries and power upper limits for this aggregator, with the results shown in **Figure 3**.

In terms of environmental and economic parameters, the carbon emission intensities for main grid electricity purchases and local DGs are set to 0.85 t/MWh and 0.50 t/MWh, respectively. The DSO implements a tiered carbon trading mechanism, setting two demarcation thresholds of 5 tons and 15 tons for the system's net emissions. The corresponding three-tier carbon trading prices are 60, 90, and 150 CNY/t, effectively guiding low-carbon operation through step-wise

penalty costs. The pricing mechanism aligns with the main grid's time-of-use (TOU) tariffs: prices during the valley periods (01:00-07:00, 23:00-24:00), flat periods, and peak periods (11:00-13:00, 19:00-21:00) are 0.3, 0.7, and 1.2 CNY/kWh, respectively.

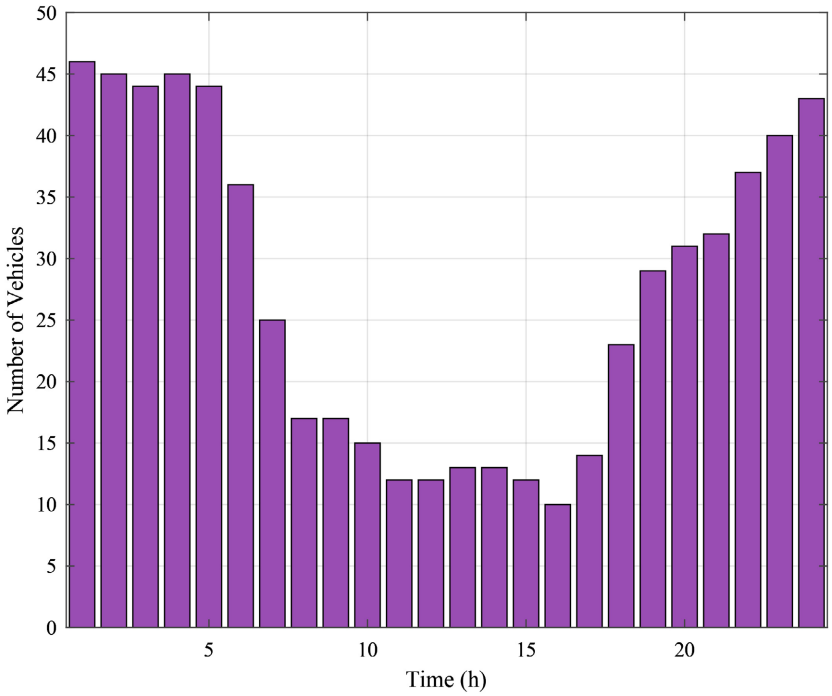

(a)

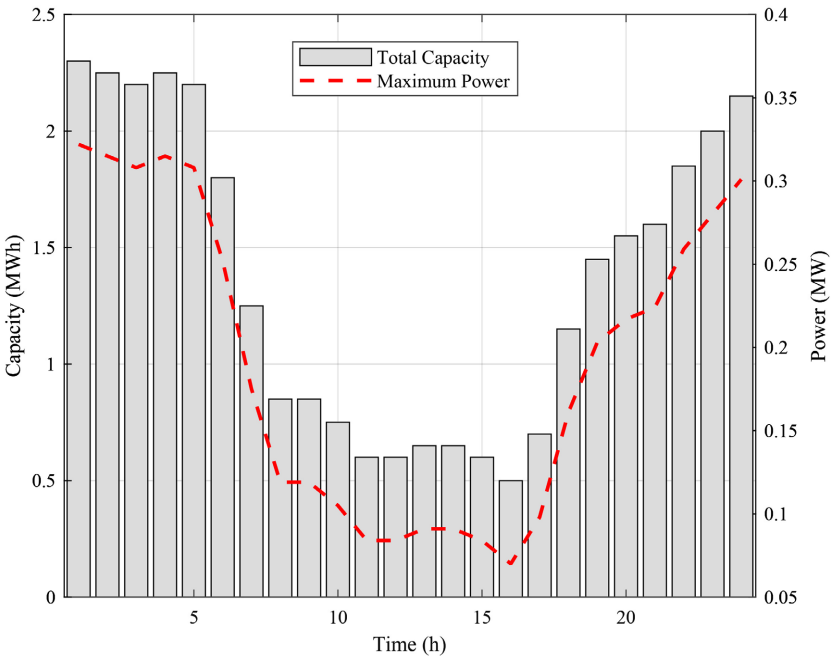

(b)

Figure 3. EV aggregator simulation results: (a) Number of online vehicles; (b) Aggregated dispatchable capacity and power upper limits.

5.2. Result Analysis

Figure 4 shows the dynamic locational marginal prices (DLMPs) at each node. The nodal DLMPs generally follow the peak-valley trend of the main grid prices. However, price divergence among nodes occurs during local peak load periods. For instance, between 11:00-13:00 and 19:00-21:00, although the main grid price rises to approximately 1.2 CNY/kWh, the marginal prices at the load aggregator nodes remain lower than the main grid price. This is because the system prioritizes resources with lower marginal costs. During these periods, the system dispatches local distributed gas generators and energy storage to meet the increased load, thereby avoiding expensive power purchases from the main grid.

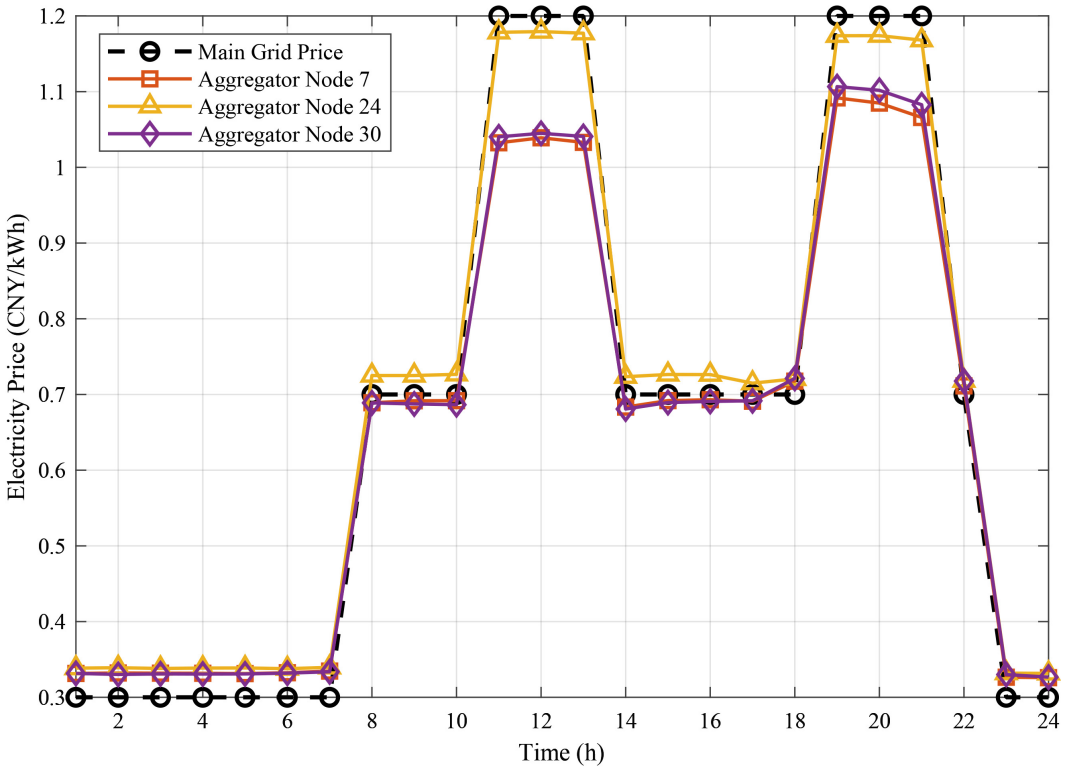

Figure 4. Comparison between the real-time distribution locational marginal prices and the main grid time-of-use prices.

Figure 5 shows the system power balance curve. Between 10:00 and 15:00, the output of photovoltaic (PV) resources significantly reduces the net load demand. During the evening peak between 19:00 and 22:00, PV output drops to zero while residential load peaks. During this period, rather than solely purchasing power from the main grid, the system relies on increased output from distributed generators (DGs), discharging of energy storage, and reverse power supply from electric vehicles (EVs). Figure 6 details the corresponding supply-side scheduling. During off-peak and flat periods, the system relies on main grid power purchases and steady DG output for the base load. During peak load periods, power purchases from the main grid are restricted within safety thresholds, and the discharge from

energy storage and EVs increases to meet the demand, which mitigates the power supply pressure on the main grid and reduces line congestion risks.

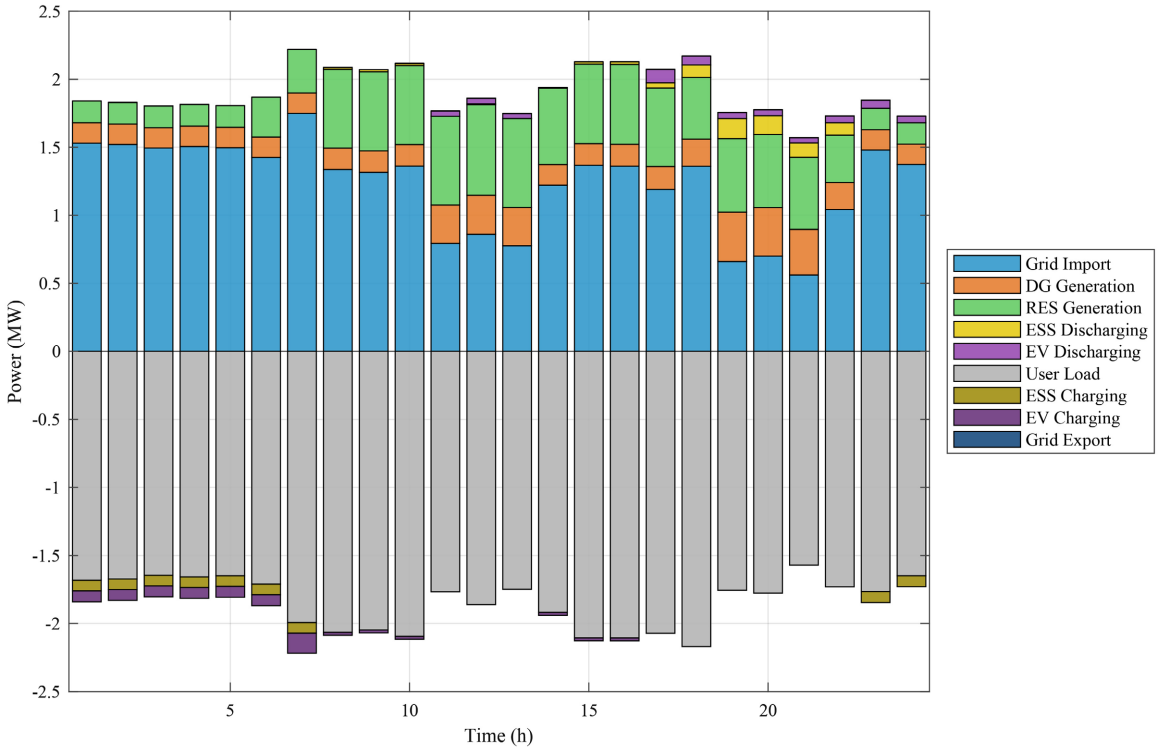

Figure 5. Total power balance of the distribution network system.

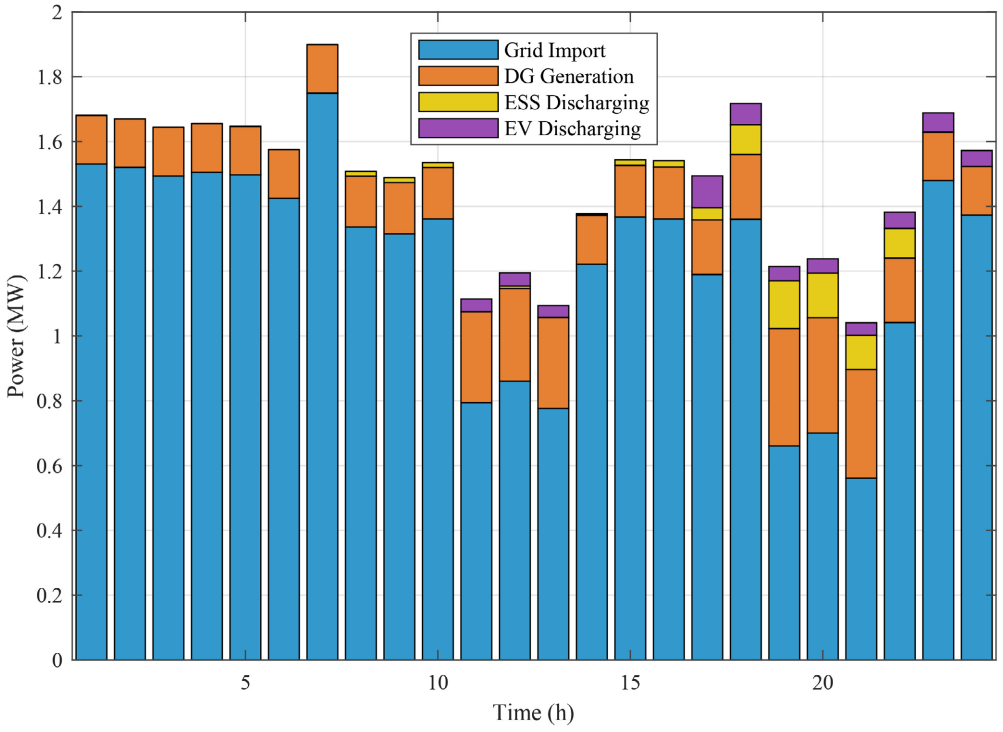

Figure 6. Optimal dispatch of the controllable supply-side resources.

Figure 7 illustrates the response of different load aggregators to the DLMPs. During peak price periods, commercial and industrial loads reduce their demand and shift flexible loads to the early morning off-peak periods or midday periods with high PV output. In contrast, residential load is relatively rigid, resulting in a limited peak-shaving capability during the evening peak, though slight adjustments in energy consumption are still observed based on the price signals.

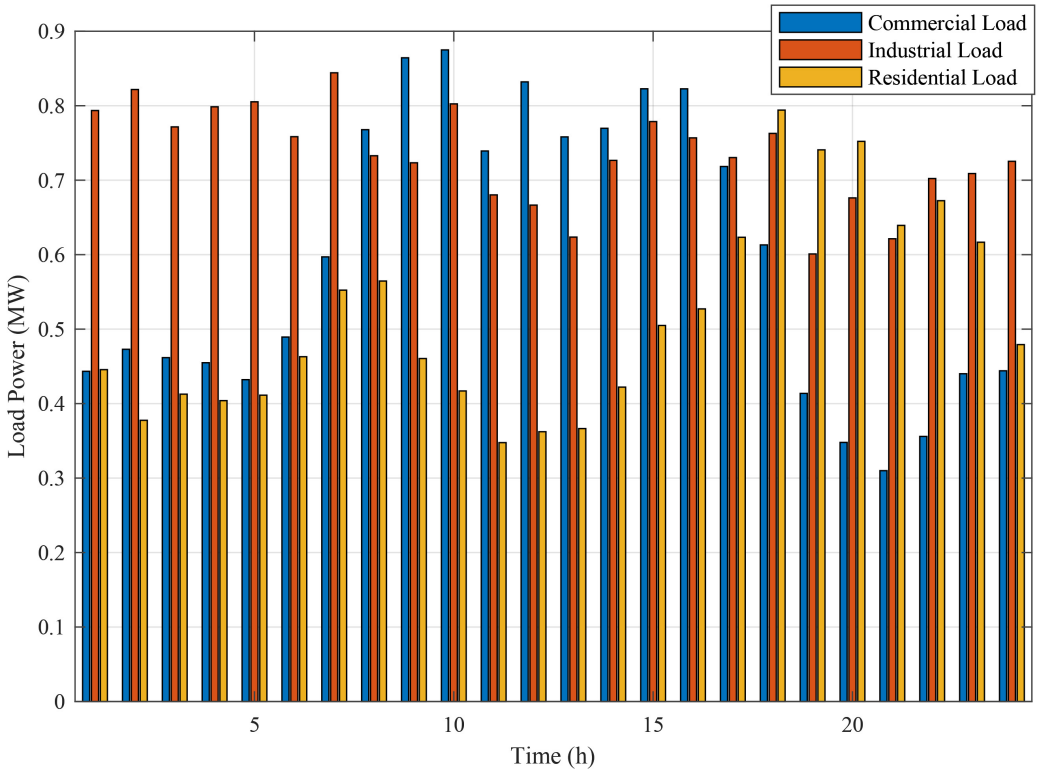

Figure 7. Optimal load response dispatched by different load aggregators

Figure 8 and Figure 9 show the optimal scheduling of independent energy storage and EV aggregators. Between 02:00 and 06:00 (the lowest price period), both charge centrally to increase their state of charge using low-priced electricity. Between 19:00 and 21:00 (the highest price period), the energy storage system discharges, and EV aggregators supply power back to the grid via V2G technology. Figure 10 shows the operation of DGs. From 01:00 to 07:00, when the electricity price is lower than the marginal generation cost, DGs operate at their minimum technical output. The negative profit during this period is an operational cost incurred to prevent frequent start-ups and shut-downs. After 08:00, DGs operate during flat and peak price periods to maximize their daily profit.

Figure 11 presents the overall social welfare of the system. The system maintains positive social welfare across all time periods, even with the inclusion of environmental constraints such as stepped carbon costs. Figure 12 compares the social welfare under the proposed DLMP mechanism and the traditional fixed price mechanism [30]. Under identical physical network constraints and equipment

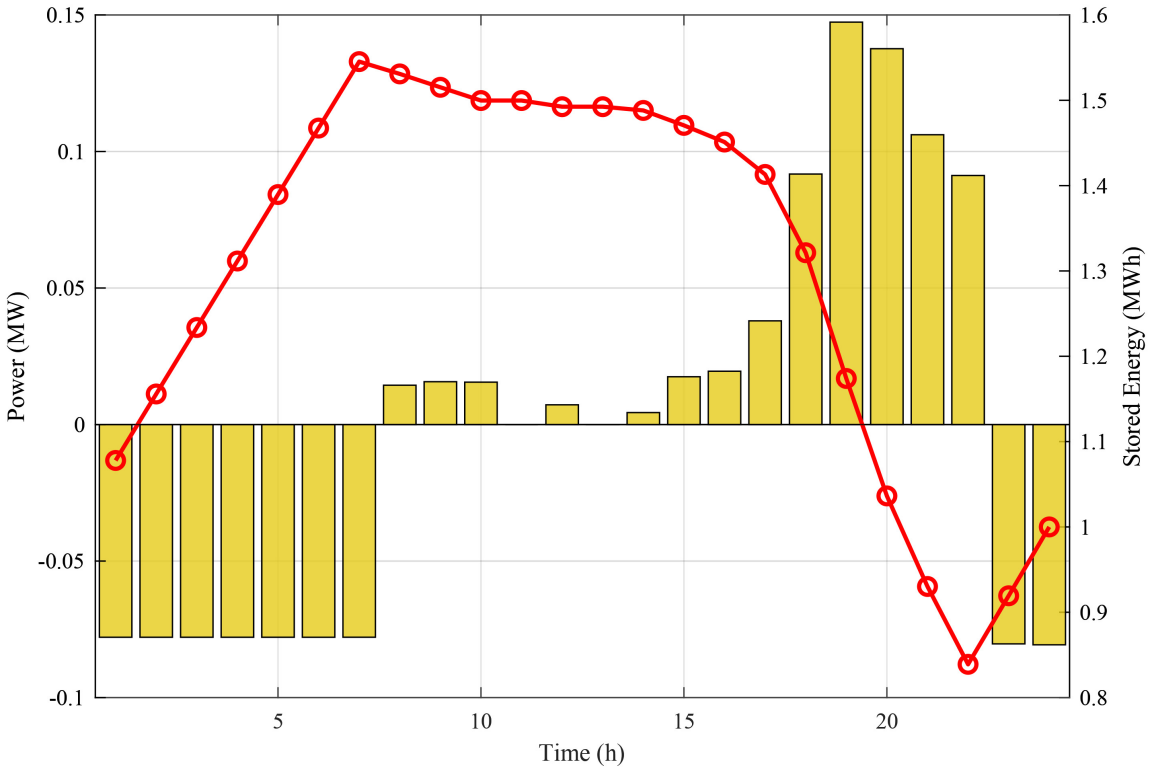

Figure 8. Optimal charging/discharging power and state of charge of the energy storage system.

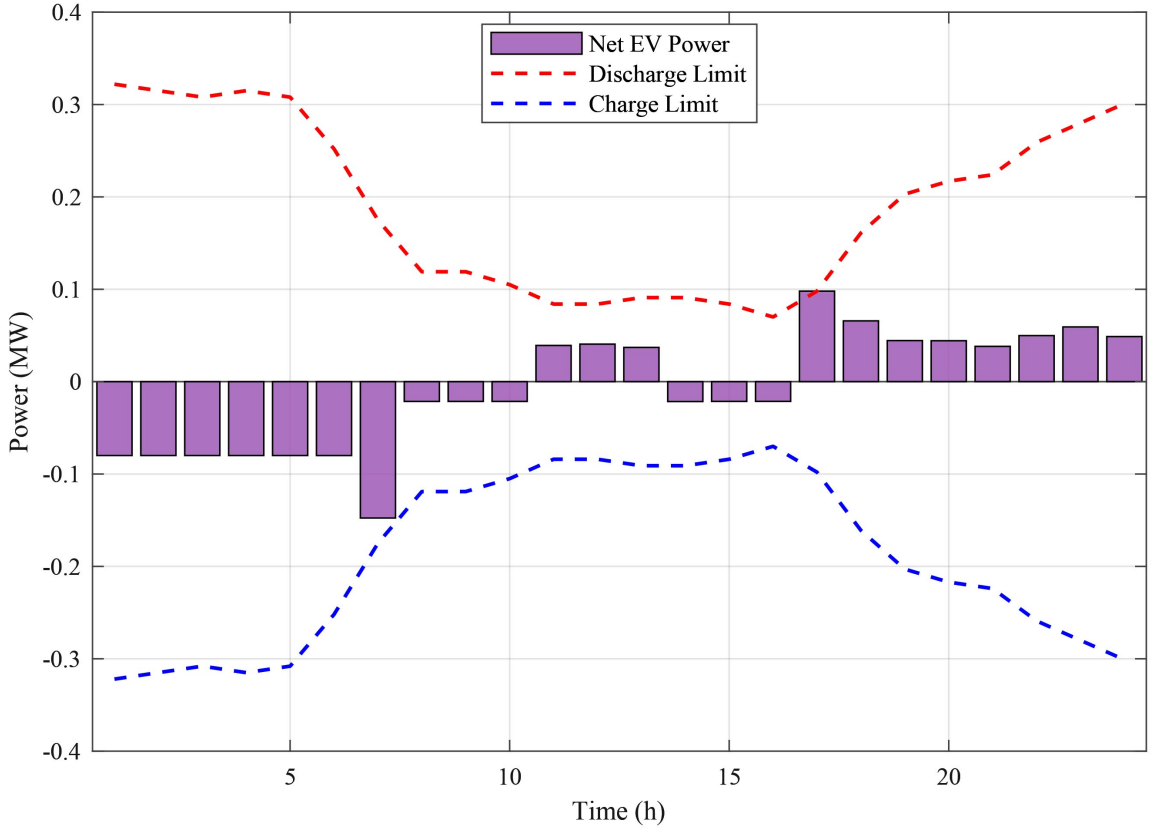

Figure 9. Optimal scheduling and operational power boundaries of the EV aggregator.

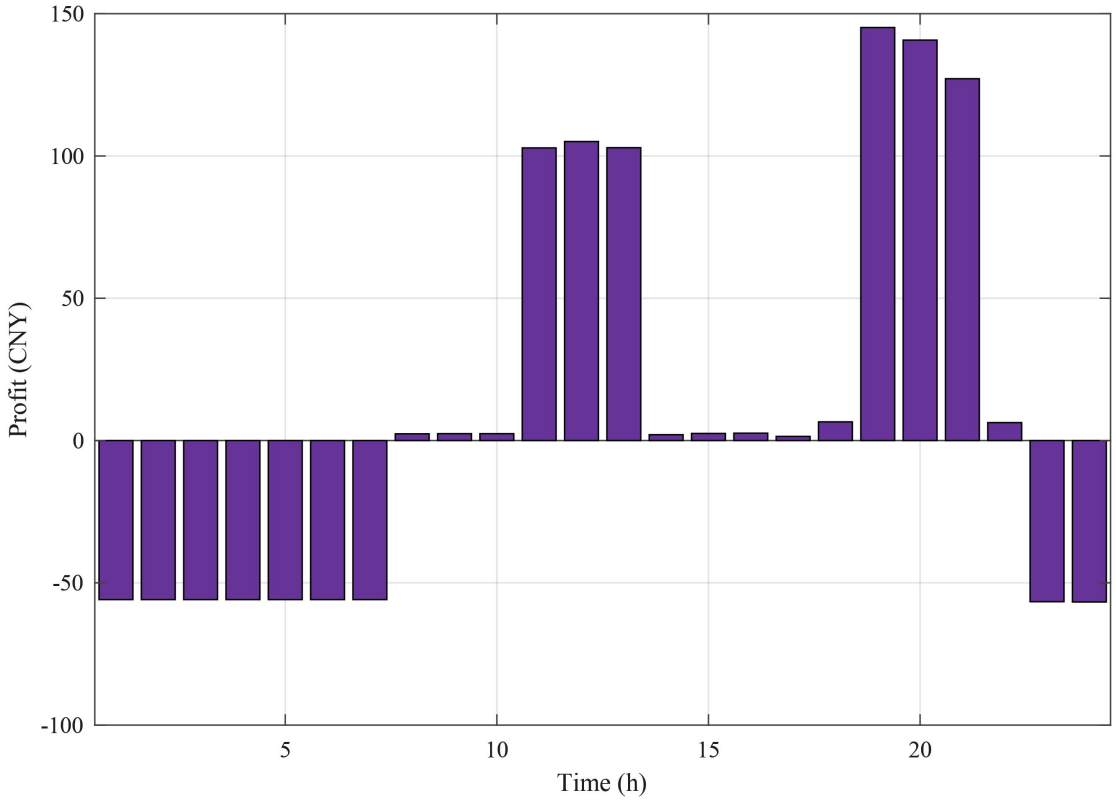

Figure 10. Hourly profit distribution of the distributed generation units.

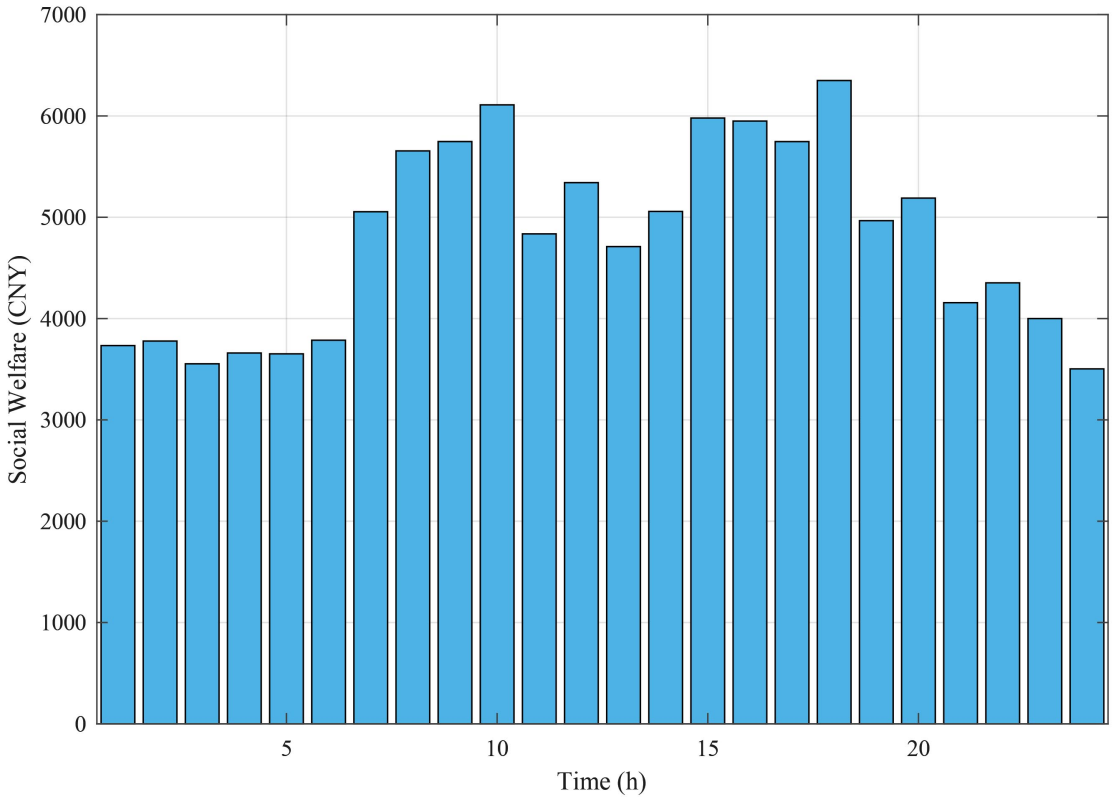

Figure 11. Hourly total social welfare of the distribution system.

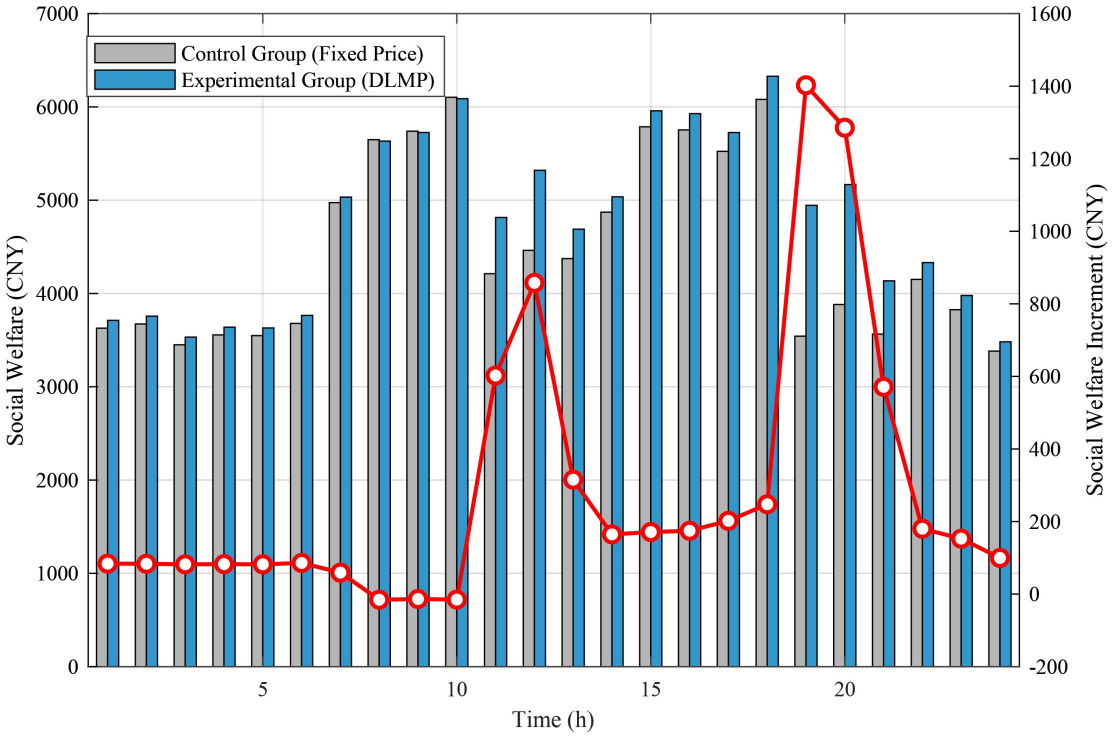

Figure 12. Comparison of system social welfare under the proposed DLMP mechanism and the traditional fixed-price mechanism.

parameters, the fixed price mechanism relies on artificially high peak prices that overly suppress flexible load, resulting in a severe loss of user utility. In contrast, the DLMP mechanism dynamically clears the market based on actual supply and demand. By fully utilizing local flexible resources and internalizing the stepped carbon costs, the DLMP avoids overly punitive price spikes and encourages load aggregators to consume electricity rationally to maximize their utility. As intuitively shown by the cumulative area under the curves in Figure 12, the proposed DLMP mechanism yields a significantly higher total social welfare over the 24-hour horizon. This macroscopic improvement robustly demonstrates that the DLMP mechanism finds the mathematically exact optimal trade-off between maximizing economic benefits and assuming environmental responsibilities, rather than blindly suppressing energy demand.

6. Conclusions

To address the net load fluctuations and physical violation risks caused by the high penetration of distributed energy resources in distribution networks, this paper proposes an optimal distribution locational marginal pricing (DLMP) strategy that considers both AC power flow constraints and a stepped carbon trading mechanism. A social welfare maximization model incorporating distributed generators, energy storage systems, and electric vehicle aggregators is established. To address the non-convex power flow constraints, the second-order cone programming (SOCP) technique is employed to transform the original model into a tractable

second-order cone programming (SOCP) problem, which strictly ensures the physical feasibility and operational security of the dispatch results. Furthermore, based on the Lagrangian dual decomposition theory, the DLMP is derived, providing a unified economic signal that comprehensively reflects the spatial-temporal dynamics of energy supply, network congestion, losses, and carbon emissions. Simulation results based on a modified IEEE 33-bus system demonstrate that the spatiotemporally differentiated price signals generated by the proposed mechanism can effectively guide flexible resources to achieve an optimal economic dispatch, mitigating nodal voltage violations and line congestion. Compared with the traditional fixed-price mechanism, the proposed strategy maximizes the overall social welfare by unlocking higher user utility while rationally internalizing the stepped carbon trading costs, which verifies its effectiveness in promoting the low-carbon synergistic optimization of "source-grid-load-storage".

Future research can be further extended in the following directions: First, considering the disturbances of multiple uncertainties (e.g., drastic renewable energy fluctuations and load forecasting errors under extreme weather) on real-time clearing prices to explore online pricing frameworks based on robust optimization or data-driven methods. Second, refining the load models with real-world data to improve the prediction accuracy of demand response.

Conflicts of Interest

The author declares no conflicts of interest regarding the publication of this paper.

References

[1] Liu, F. and Ma, T.J. (2025) Review and Frontier Prospect of the Researches on the Mechanisms and Strategies of Wind and Solar Power Consumption. *Chinese Journal of Management Science*, **33**, 247-258.

[2] Wang, Y., Li, J., Gao, Y., Xu, H., Dong, J., Qu, D., *et al.* (2025) Process Monitoring and Adjustment Method with Application to Real-Time Electricity and Internal Carbon Pricing Models under Reputation Theory. *Energy Economics*, **152**, Article ID: 108983. https://doi.org/10.1016/j.eneco.2025.108983

[3] Zhao, Z., Liu, Y., Guo, L., Bai, L., Wang, Z. and Wang, C. (2023) Distribution Locational Marginal Pricing under Uncertainty Considering Coordination of Distribution and Wholesale Markets. *IEEE Transactions on Smart Grid*, **14**, 1590-1606. https://doi.org/10.1109/tsg.2022.3200704

[4] Li, N. and Gao, Y. (2023) Real-time Pricing Based on Convex Hull Method for Smart Grid with Multiple Generating Units. *Energy*, **285**, Article ID: 129543. https://doi.org/10.1016/j.energy.2023.129543

[5] Haider, R., D'Achiardi, D., Venkataramanan, V., Srivastava, A., Bose, A. and Annaswamy, A.M. (2021) Reinventing the Utility for Distributed Energy Resources: A Proposal for Retail Electricity Markets. *Advances in Applied Energy*, **2**, Article ID: 100026. https://doi.org/10.1016/j.adapen.2021.100026

[6] Li, M. and Ahad, Y. (2023) A Novel Real-Time Pricing for Optimal DRP, Considering Price Elasticity, and Charging Control Methods of PHEV Integrated with Smart Grids, Using GMO Algorithm. *Engineering Science and Technology, an International Journal*, **47**, Article ID: 101538. https://doi.org/10.1016/j.jestch.2023.101538

[7] Gao, Y. (2022) Review of Real-Time Electricity Price Optimization Methods Based on Demand Side Management. Journal of University of Shanghai for Science and Technology, 44, 103-111. https://doi.org/10.13255/j.cnki.jusst.20220328004

[8] Hogan, W.W. (2014) Electricity Market Design and Efficient Pricing: Applications for New England and Beyond. *The Electricity Journal*, **27**, 23-49. https://doi.org/10.1016/j.tej.2014.07.009

[9] Wang, X.Y., Gao, F., Kang, C.Q. (2019) Research on Extended Locational Marginal Pricing Algorithm. Power System Technology, 43, 3587-3596. https://doi.org/10.13335/j.1000-3673.pst.2018.3038

[10] Tan, Z., Cheng, T., Liu, Y. and Zhong, H. (2022) Extensions of the Locational Marginal Price Theory in Evolving Power Systems: A Review. *IET Generation*, *Transmission & Distribution*, **16**, 1277-1291. https://doi.org/10.1049/gtd2.12381

[11] Pandey, V.C., Rawat, T., Ospina, J., Dvorkin, Y. and Konstantinou, C. (2025) A Tri-Level Distribution Locational Marginal Price-Based Demand Response Framework. *Electric Power Systems Research*, **241**, Article ID: 111398. https://doi.org/10.1016/j.epsr.2024.111398

[12] Mieth, R. and Dvorkin, Y. (2020) Online Learning for Network Constrained Demand Response Pricing in Distribution Systems. *IEEE Transactions on Smart Grid*, **11**, 2563-2575. https://doi.org/10.1109/tsg.2019.2957705

[13] Zhang, J., Li, X.Q. and Wei, Y.D. (2025) Improved Model of Ultimate Power Supply Capacity of VSC-HVDC Traction Power Supply System Based on SOCP. *Proceedings of the CSEE*, **45**, 813-822.

[14] Alsaleh, I. and Alassaf, A. (2024) Optimizing Local Electricity Markets: A Bi-Level Primal-Dual Approach for Integrating Price-Based Demand Response and Distribution Locational Marginal Pricing. *Ain Shams Engineering Journal*, **15**, Article ID: 102929. https://doi.org/10.1016/j.asej.2024.102929

[15] Zhu, H., Gao, Y., Hou, Y., Wang, Z. and Feng, X. (2019) Real-time Pricing Considering Different Type of Smart Home Appliances Based on Markov Decision Process. *International Journal of Electrical Power & Energy Systems*, **107**, 486-495. https://doi.org/10.1016/j.ijepes.2018.12.002

[16] Wu, Z.Q., Wang, J.Q. and Gao, Y. (2024) Social Welfare Analysis of Real-Time Electricity Pricing. *Chinese Journal of Management Science*, **32**, 218-227.

[17] Yang, Z. and Qin, Z. (2023) Demand Response Model by Locational Marginal Electricity–carbon Price Considering Wind Power Uncertainty and Energy Storage Systems. *Energy Reports*, **9**, 742-752. https://doi.org/10.1016/j.egyr.2023.04.209

[18] Luo, Y., Gao, Y. and Fan, D. (2023) Real-time Demand Response Strategy Base on Price and Incentive Considering Multi-Energy in Smart Grid: A Bi-Level Optimization Method. *International Journal of Electrical Power & Energy Systems*, **153**, Article ID: 109354. https://doi.org/10.1016/j.ijepes.2023.109354

[19] Zhang, Y.W., Wu, H.Q. and Wan, H.Y. (2023) Reliability Assessment of Regional Integrated Energy System Considering with Multiple Thermal Inertia Characteristics. *Transactions of China Electrotechnical Society*, **38**, 3289-3305.

[20] Feng, C., Li, Z., Shahidehpour, M., Wen, F. and Li, Q. (2020) Stackelberg Game Based Transactive Pricing for Optimal Demand Response in Power Distribution Systems. *International Journal of Electrical Power & Energy Systems*, **118**, Article ID: 105764. https://doi.org/10.1016/j.ijepes.2019.105764

[21] Luo, Y. and Gao, Y. (2025) Real-time Pricing Strategy Considering Carbon Emissions and Time Coupling in Smart Grid: A Binary Integer Bilevel Optimization Model with

Decision-making. *Engineering Applications of Artificial Intelligence*, **141**, Article ID: 109858. https://doi.org/10.1016/j.engappai.2024.109858

[22] Que, Y.L. (2024) Nodal Real-Time Pricing Strategy for Multi-User and Multi-Supplier in Smart Grid Based on ADMM. *Pure Mathematics*, **14**, 104-114.

[23] Zhang, L., Gao, Y., Liu, S.T. and Zhu, H.B. (2019) Multi-Time Slots Real-Time Pricing for Smart Grid with Time-Coupled Constraints. *Systems Engineering—Theory & Practice*, **39**, 2599-2609.

[24] Song, H., Wang, Z. and Gao, Y. (2025) Bi-Level Real-Time Pricing Model in Multi-type Electricity Users for Welfare Equilibrium: A Reinforcement Learning Approach. *Journal of Renewable and Sustainable Energy*, **17**, Article ID: 015501. https://doi.org/10.1063/5.0242836

[25] Albadi, M.H. and El-Saadany, E.F. (2008) A Summary of Demand Response in Electricity Markets. *Electric Power Systems Research*, **78**, 1989-1996. https://doi.org/10.1016/j.epsr.2008.04.002

[26] Lyu, C., Jia, Y. and Xu, Z. (2021) Fully Decentralized Peer-To-Peer Energy Sharing Framework for Smart Buildings with Local Battery System and Aggregated Electric Vehicles. *Applied Energy*, **299**, Article ID: 117243. https://doi.org/10.1016/j.apenergy.2021.117243

[27] Rigo-Mariani, R. and Vai, V. (2022) An Iterative Linear Distflow for Dynamic Optimization in Distributed Generation Planning Studies. *International Journal of Electrical Power & Energy Systems*, **138**, Article ID: 107936. https://doi.org/10.1016/j.ijepes.2021.107936

[28] Farivar, M. and Low, S.H. (2013) Branch Flow Model: Relaxations and Convexification—part I. *IEEE Transactions on Power Systems*, **28**, 2554-2564. https://doi.org/10.1109/tpwrs.2013.2255317

[29] Gan, L., Li, N., Topcu, U. and Low, S.H. (2014) Exact Convex Relaxation of Optimal Power Flow in Radial Networks. *IEEE Transactions on Automatic Control*, **60**, 72-87.

[30] Samadi, P., Mohsenian-Rad, A., Schober, R., Wong, V.W.S. and Jatskevich, J. (2010) Optimal Real-Time Pricing Algorithm Based on Utility Maximization for Smart Grid. 2010 *First IEEE International Conference on Smart Grid Communications*, Gaithersburg, 4-6 October 2010, 415-420. https://doi.org/10.1109/smartgrid.2010.5622077